Solar Energy 224 (2021) 1313–1325

Contents lists available at ScienceDirect

Solar Energy

journal homepage: www.elsevier.com/locate/solener

Improved thermo-economic performance of solar desalination via copper chips, nanofluid, and nano-based phase change material

A.W. Kandeal [a,b], Nagi M. El-Shafai [c], Mohamed R. Abdo [d], Amrit Kumar Thakur [e], Ibrahim M. El-Mehasseb [c], Ibrahem Maher [b], Maher Rashad [f], A.E. Kabeel [g,h], Nuo Yang [a,*], Swellam W. Sharshir [a,b,*]

[a] School of Energy and Power Engineering, Huazhong University of Science and Technology, Wuhan 430074, China
[b] Mechanical Engineering Department, Faculty of Engineering, Kafrelsheikh University, Kafrelsheikh 33516, Egypt
[c] Nanotechnology Center, Chemistry Department, Faculty of Science, Kafrelsheikh University, 33516, Egypt
[d] Department of Engineering Mathematics and Physics, Faculty of Engineering, University of Kafrelsheikh, Kafrelsheikh, Egypt
[e] Department of Mechanical Engineering, KPR Institute Engineering and Technology, Coimbatore, Tamilnadu, India
[f] Production Engineering and Mechanical Design Department, Faculty of Engineering, Tanta University, Egypt
[g] Mechanical Power Engineering Department, Faculty of Engineering, Tanta University, Tanta, Egypt
[h] Faculty of Engineering, Delta University for Science and Technology, Gamasa, Egypt

ARTICLE INFO

Keywords:
Solar desalination
Nanofluids
Copper chips
Energy efficiency
Exergy efficiency
PCM

ABSTRACT

In this work, the performance of a modified double slope still (MDSSS) was evaluated compared to conventional single slope one (CSS). The modifications depended on different additives, namely: copper chips, copper oxide (CuO) nanoparticles/fluid, and paraffin wax as phase change material (PCM). First, the proposed materials were characterized to determine the thermophysical properties and the best ratios. As resulted, the copper chips, and nano-enhanced materials (water and PCM) had higher thermal conductivity than bulk water, and pure materials, respectively. Beyond the characterization, three cases of MDSSS were investigated compared to CSS: copper chips immersed in CuO/water nanofluid (1.5 wt%) (case I), integrating pure PCM container below the basin containing the previous materials (case II), and using nano-based PCM (15 wt%) instead of the pure PCM (case III). Moreover, the thermo-economic performance was evaluated by determining the efficiencies of the first and second laws of thermodynamics and the freshwater cost. As found, all cases showed good performance improvements, and case III was the best from both production and thermo-economic considerations. For this case, the productivity, energy efficiency, and exergy efficiency were enhanced by 113, 112.5, and 190%, respectively, relative to CSS. In addition, the freshwater production cost was saved by 35.3%.

1. Introduction

Recently, along with the increasing population, industrial growth, and pollution, the world is facing freshwater scarcity as only 0.014% of the total water that exists on Earth is available for humans and other living organisms (Bendfeld et al., 1998). In other words, about 97.5% of the globe's water bodies represent saltwater, and the remaining 2.5% is freshwater. Unfortunately, most of this small freshwater amount exists in polar ice, atmosphere, and groundwater, whereas the minority is reachable water (Abujazar et al., 2018). Hence, about 33% of the globe's population has difficulties reaching drinkable water and deadly faces freshwater shortage scarcity, especially with the lack of energy sources required for water desalination (Thimmaraju et al., 2018). Fortunately, the solar radiation intensity covers almost all the Earth surface with an average daily intensity that varies from 2.2 to 74 kWh/m^2 (Sharshir et al., 2020b). Hence, it is a great opportunity to enlarge the field of eco-friendly solar desalination techniques. There are many types of solar-powered desalination units, such as solar still (SS) (Sharshir et al., 2016c), humidification-dehumidification (HDH) (Hamed et al., 2015; Kabeel et al., 2013, 2014), multi-stage flashing (Alsehli et al., 2017), reverse osmosis (RO) (Elkadeem et al., 2021; Elmaadawy et al., 2020b; Kotb et al., 2021), and hybrid units (Abdelgaied et al., 2021; Sharshir et al., 2016a, 2016b).

Among all solar-driven desalination techniques, SS has become a

* Corresponding authors at: School of Energy and Power Engineering, Huazhong University of Science and Technology, Wuhan 430074, China.
E-mail addresses: nuo@hust.edu.cn (N. Yang), sharshir@eng.kfs.edu.eg (S.W. Sharshir).

https://doi.org/10.1016/j.solener.2021.06.085
Received 4 February 2021; Received in revised form 26 June 2021; Accepted 30 June 2021
Available online 8 July 2021

promising and feasible one, especially for remote areas that require small freshwater production (Sharshir et al., 2017a, 2020f). SSs have been preferred for many advantages: simple installation, low cost and easy operation, low need for labor, and eco-friendly. Contrary, the low yield and efficiency are the main demerits of SSs, which the recent research works have aimed to improve via different techniques (Abdelaziz et al., 2021; Elshamy and El-Said, 2018; Sathyamurthy et al., 2020; Shalaby et al., 2016; Sharshir et al., 2016c). Based on surveyed works, the majority of these efforts have focused on improving the thermal design, which can be enhanced either by changing the still design (especially transparent cover) or using additives (externally or internally).

The SS cover design can be changed to collect more solar radiation needed to increase the evaporation rate. Along with that, various designs have been developed and tested, such as double slope SS (DSSS) (Morad et al., 2015; Patel et al., 2020), pyramid SS (Kabeel et al., 2020), and tubular SS (Sharshir et al., 2019a; Wang et al., 2020). Also, SSs can be attached to external additives/devices that help in increasing the evaporation and condensation rates, which is known as "active SSs," utilizing: external condenser (Ali, 1991), solar collectors (Tanaka and Nakatake, 2009; Voropoulos et al., 2003), sun-tracking system (Abdallah and Badran, 2008), glass cooling units (Sharshir et al., 2017b), etc. Moreover, the internal design of the SS can be improved either by using different absorber designs (Arunkumar et al., 2018; Madani and Zaki, 1995; Samuel Hansen and Kalidasa Murugavel, 2017) or using additives, such as sponge cubes (Rababa'h, 2003), black gravels (Nafey et al., 2001), black rubber/gravel mixture (Khare et al., 2017), heat localization materials (Sharshir et al., 2020g), sand/steel mixture (Hassan and Abo-Elfadl, 2017), etc. Among the internal additives, the current work focused on phase change materials (PCMs), and nanofluids/particles.

Utilizing PCMs, the SS performance can be enhanced as the heat is stored during the charging process to be used in late hours when solar radiation is low; hence the process can continue for many hours that may extend to the night (Sharshir et al., 2019c). Taking this advantage, many efforts have been conducted to improve the SSs' performance by attaching PCMs in various orientations (El-Sebaii et al., 2009; Kabeel et al., 2018, 2017; Mousa and Gujarathi, 2016; Radhwan, 2005; Su et al., 2015). Paraffin wax has been commonly used in SSs because it has a convenient melting point temperature and high latent heat of fusion, however, its main disadvantage is its low thermal conductivity. It showed a good enhancement of single slope SS's yield by 68.8%, according to the experiments done by Kabeel and Abdelgaied (2016).

Recently, with the development of nanotechnology applications in thermal systems, nano-based SSs have been investigated (El-Shafai et al., 2021; Elsheikh et al., 2019; Kabeel et al., 2019; Peng et al., 2020, 2018, 2021; Rashidi et al., 2018; Sharshir et al., 2020a, 2020c, 2020d, 2019b, 2018, 2017c; Thakur et al., 2021). Additions of nanoparticles to base materials enhance the thermal properties without significant change of specific heat, such as in the case of nanofluids (Choi and Eastman, 1995). Different nanomaterials have been integrated into SSs, and the results were satisfying with productivity increase by about 29.95, 18.63, and 12.67% using aluminum oxide (Al_2O_3), tin oxide (SnO_2), and zinc oxide (ZnO) nanofluids, respectively (Elango et al., 2015). Furthermore, nano-based PCMs have been developed to enhance the thermal conductivity of PCM, which is a major demerit, as previously mentioned (Dsilva Winfred Rufuss et al., 2018; Sharshir et al., 2021).

Herein, the current work aimed to investigate the developed thermal design of SS either by changing the still design itself or using internal additives. For this aim, the thermo-economic performance of DSSS integrated sensible heat bed, nanofluid, and PCM was investigated compared to conventional SS (CSS). The sensible bed was fabricated from copper chips and added to the basin area immersed in copper-oxide (CuO) nanofluid. Also, a pure and nano-based paraffin wax container was attached to the basin bottom as a latent heat bed. For a comprehensive study, the following highlighted procedures were conducted:

i. The thermophysical properties of the proposed materials (CuO nanofluid, pure, and nano-based PCM) were characterized. According to that, the best concentration of CuO in paraffin wax was selected based on the highest thermal conductivity, which was 15 wt%.
ii. The effect of the copper chips layer immersed in CuO nanofluid on the DSSS performance was evaluated (Case I).
iii. Pure paraffin (pure PCM) container was attached to the basin of the previous case and performance was experimented with (Case II).
iv. A nano-based PCM container was used instead of the pure one (Case III).
v. The thermo-economic performance for all cases was analyzed by calculating the energy efficiency, exergy efficiency, and production cost per unit liter.

During each experiment, all performance affecting parameters (solar radiation, wind speed, and temperatures of water, glass, and ambient) as well as the productivity were recorded hourly for both modified DSSS (MDSSS) and CSS simultaneously. All characterization, experimental and analytical data are presented in detail.

2. Thermo-physical properties of proposed materials

The proposed materials, especially CuO nanoparticles and nano-based PCM, were characterized before integrating them within the DSSS. The surface characterizations of CuO and nano-based PCM were obtained via different methods, namely: Scanning electron microscopy (SEM), high-resolution Transmission electron microscopy (TEM) images, X-ray diffraction (XRD) measurements, and ultraviolet tests. Besides, the thermal conductivity of pure and nano-based paraffin wax (at different concentrations) was measured. The following sections discuss the obtained characterization results.

2.1. Surface characterization of CuO nanoparticles, pure PCM, and nano-based PCM

The SEM, and TEM images at different magnifications and the Energy-dispersive X-ray spectroscopy (EDS) analyses are shown in Figs. 1 and 2 for pure CuO, and nano-based paraffin wax, respectively. As shown, the morphological details for CuO appeared as a nanorod shape with approximately 8 nm width and 40 nm length. The observed average size matched the value that was calculated from the XRD item, as furtherly discussed. The structural details revealed the absence of any pattern peaks of other elements except CuO patterns; also, the morphological details and EDS analysis have illustrated the formation of the pure CuO nanorods. On the other hand, for nano-based paraffin wax, Fig. 2, there was no distinct difference noticed in the shape and morphology of pure CuO, probably because the CuO particles were very small. It was also observed that the CuO nanorods were uniformly and homogenously distributed among paraffin wax layers, and some were concentrated in the down-faced of paraffin wax. As illustrated in the EDS results of nano-based parrafin wax, the distribution of CuO between the paraffin wax layers was confirmed, where C, N, and O percentage in pure paraffin wax and their percentage in the nano-based PCM confirmed the formation of the hybrid materials. The lattice fringes of CuO images exhibited in Fig. 1(a), which were parallel to the edges of CuO and assembled alongside one direction and no different direction that illustrated the CuO was synthesized as pure nanomaterials.

Besides, the XRD measurements of pure CuO, pure paraffin wax, and nano-based paraffin wax were conducted as presented in Fig. 3. The XRD data was reported, where a = 4.689 Å, b = 3.420 Å, c = 5.133 Å, and β = 99° 24. CuO nanorod patterns are (32.37°, 35.62°, 39.13°, 43.15°, 48.93°, 53.95°, 58.23°, 61.75°, 66.52°, 72.54°, and 75.31°) (El-Shafai et al., 2020; Lanje et al., 2010). The main grain size of CuO nanorod was calculated from the Debye-Scherrer's formula ($D = K\lambda/\beta\cos\theta$) (El-Shafai

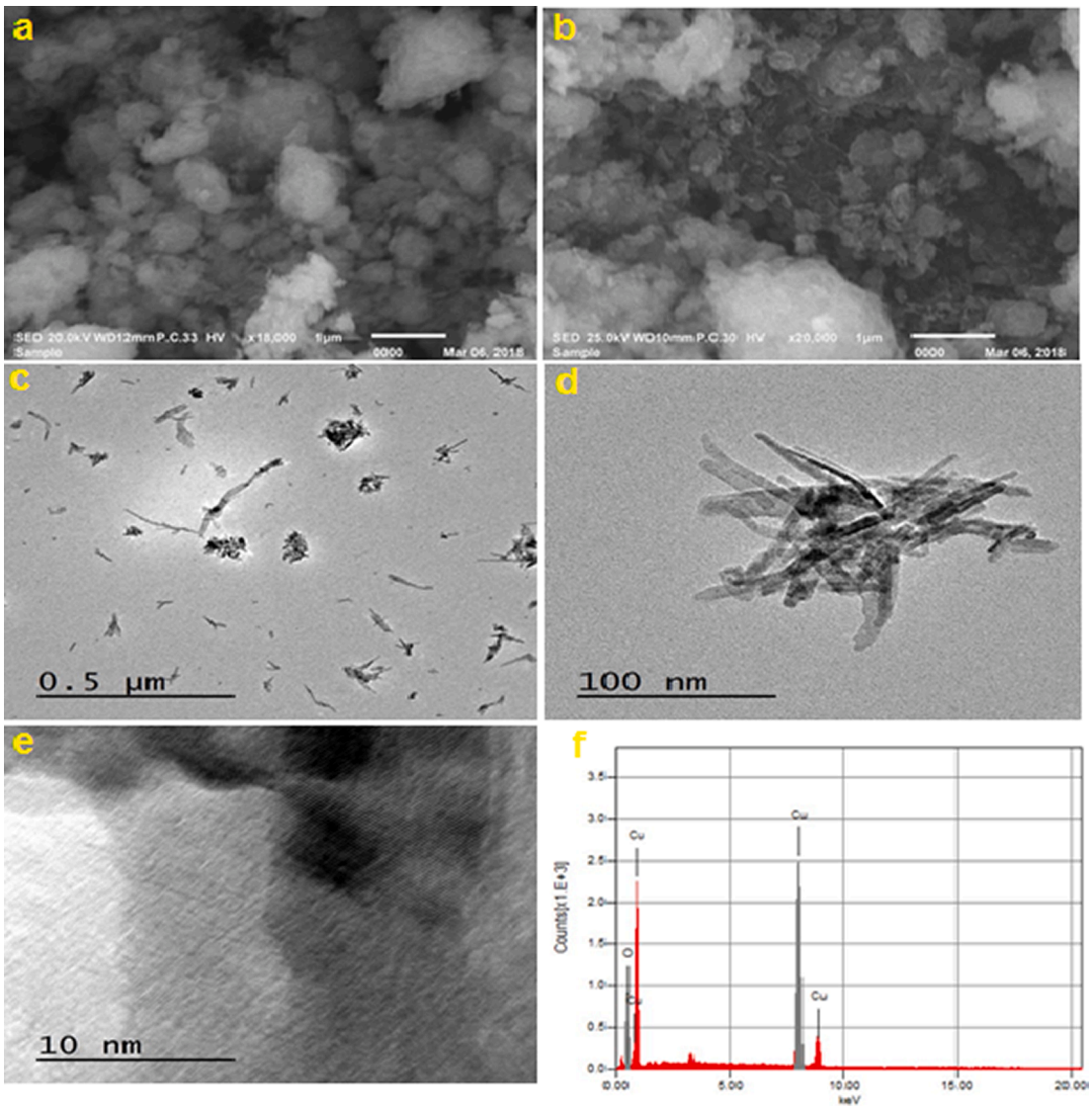

Fig. 1. Electron microscopy images of pure CuO: (a and b) SEM images, (c and d) TEM images, (e) lattice spaced-space, (f) and EDS analysis of CuO nanorod.

et al., 2020). As a result, the average crystallite sizes were determined to be 8 nm, accompanied by the values estimated from the TEM analysis. Also, the XRD pattern of paraffin wax was documented at 6.93°, 9.03°, 21.21°, and 23.7°. The nano-based paraffin wax hybrid nanocomposite with a two-faced sample gave XRD patterns matching with the patterns of pure paraffin wax, which confirmed that the CuO nanorods had a good distribution between the layers of paraffin wax, but not on the surface. Moreover, as shown in Fig. 4, the crystallinity was performed under conditions of K parameter 1, crystal Icr is 10 to 12.9629, (kcps*deg) amorphous Ia was 4.6107 to 25 (kcps*deg). The crystallinity of paraffin wax was 94%, whereas the addition of CuO nanorod did not affect the crystallinity of paraffin wax, and a small distortion (86–89%) occurred due to the addition of CuO between the crystals of paraffin wax. These data confirmed no chemical interaction between CuO and paraffin wax, but CuO NPs could groove between paraffin wax crystals.

Furthermore, the ultraviolet properties, shown in Fig. 5, of pure paraffin wax, nano-based paraffin wax (deep brown face), and nano-based paraffin wax were measured with reflectance mode under room temperature with reflectance values of 28%, 48.5%, and 61%, respectively. The bandgaps were 2.8 for (Paraffin wax), and 1.5 for (nano-based paraffin wax (deep brown face), and nano-based Paraffin wax). As a result, with the presence of CuO nanorods, the reflectance property was increased, so the nano-based PCM did not need a large amount of energy to absorbance and storage it, so this nano-based material can give high efficiency in water distillation and storage in all the time of day.

2.2. Thermal conductivity of pure, and nano-based PCM

2.2.1. Methodology, and procedures

The thermal conductivity of pure and nano-based paraffin wax (at different nanoparticle concentrations) was measured via a hot disk thermal constants analyzer, based on the thermal transient plane source (TPS) method. This method is a non-destructive technique that has been widely utilized for perfect measuring of thermal properties (conductivity, diffusivity, and specific heat) of approximately all kinds of materials. Also, it can determine the bulk, and directional properties of homogeneous and heterogeneous, and anisotropic materials, respectively.

Herein, in this works, TPS 2500 S analyzer, shown in Fig. 6, was used (range 0.005–1800 W/m K) to measure the thermal conductivity of PCM. The operation of this analyzer depended on placing a transiently heated sensor (C7577) between two sample layers. The sensor consists of a double spiral electrically conducting pattern fabricated from thin metallic foil (Nickel) and sandwiched between two thin insulating sheets (Mica, Kempton, etc.). Besides, this sensor works as a heat source and resistance thermometer at the same time, as when electricity is actuated, the temperature increase (1–7 °C), and the resistance is simultaneously

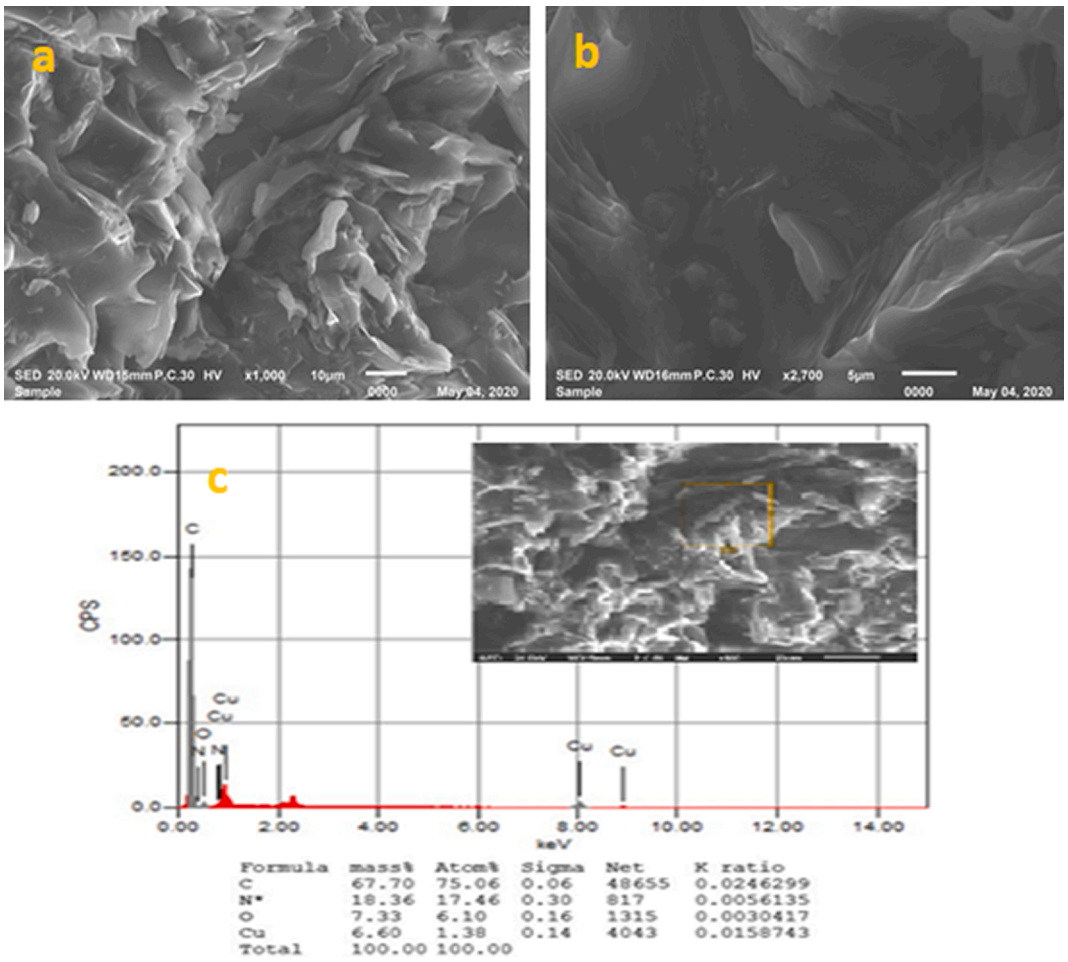

Fig. 2. Characterization of nano-based paraffin wax: (a, b) SEM images, and (c) EDS analysis.

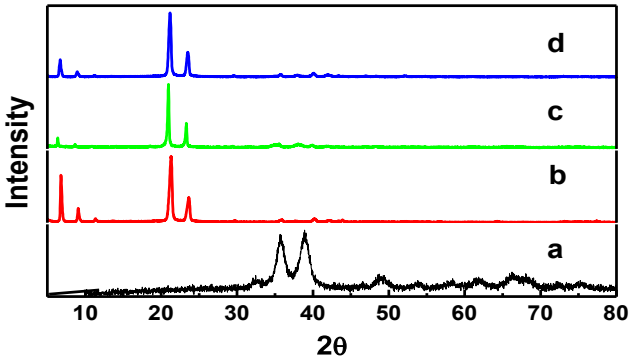

Fig. 3. XRD patterns: (a) pure CuO nanorod, (b) paraffin wax, (c) nano-based paraffin wax (deep brown face), and (d) nano-based paraffin wax.

recorded a time function. The thermal conductivity can be obtained based on the transported amount of heat per unit time through the unit area and thickness of the material.

2.2.2. Measured thermal conductivity

The resulted values of thermal conductivity measurement of both pure, and nano-based PCMs are presented in Fig. 7. As noticed, the pure paraffin wax had a low thermal conductivity of 0.214 W/m K, which was enhanced with the increased concentration of nanomaterial. It reached 0.342 W/m K at 15 wt% concentration with an enhancement ratio of ~60%. Due to high thermal conductivity, the nano-based PCM (15 wt%) was selected for the third case in the current work.

3. Experimental setup, procedures, and instrumentation

3.1. System description, and procedures

The experimental test-rig was set up on the shore of Burullus lake (a brackish lake located in the north shore of Nile River delta, Kafrelsheikh, Egypt), from which the brackish was collected (latitude 31.07°N, and longitude 30.57°E). The experiments were conducted during July and August 2020 from 8:00 to 18:00.

As presented in Fig. 8, the proposed system contained SSs; namely: single slope (conventional) SS (CSS), and modified double slope SS (MDSSS), utilized as a reference, and modified SSs, respectively. Both were fabricated from a 1.5 mm-thick, black-painted galvanized iron sheet forming a rectangular basin of 0.5 m^2 (1 × 0.5 m) area. The whole sides, except the upper glazed one, were insulated via 5 cm-thick foam that has poor thermal conductivity (~0.03 W/m K) to eliminate heat losses to the ambient. The upper lids were made from 3 mm-thick ordinary glass (emissivity = 0.88, and absorptivity = 0.05) that was tilted at 31° to the horizontal. Also, the two SSs were connected to the feed water tank (200 L) through branched pipelines with proper fittings to conserve a constant amount of water inside the SSs (5 L). Both SSs were oriented in different directions to receive the maximum possible radiation during the day; hence, MDSSS and CSS were oriented in West-East, and South directions, respectively (Sharshir et al., 2020e).

For conducting the aimed modifications on the MDSSS, non-uniform copper chips were collected from machining workshops and placed to

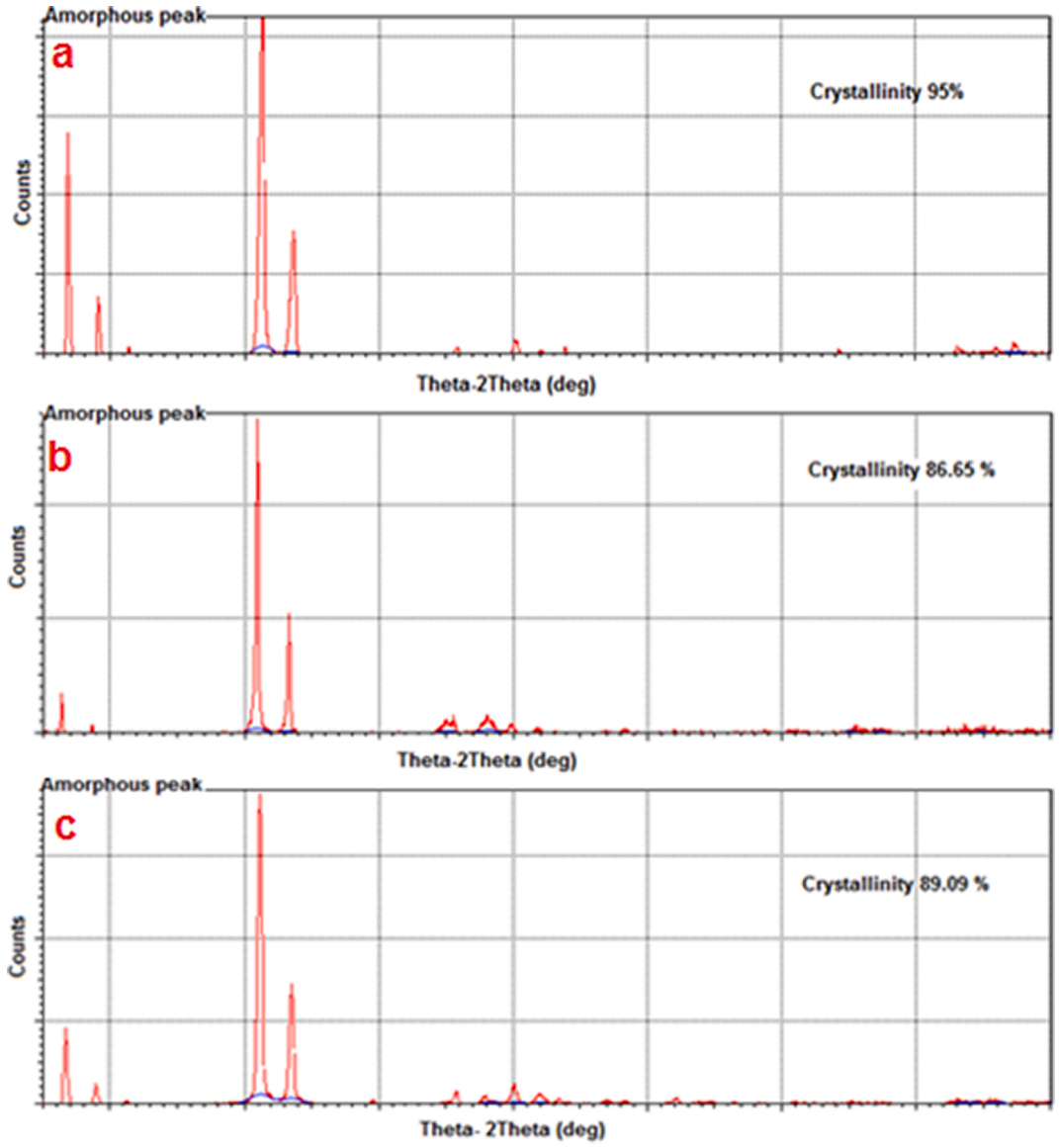

Fig. 4. The crystallinity: (a) paraffin wax, (b) nano-based paraffin wax (deep brown face), and (c) nano-based paraffin wax (brown face).

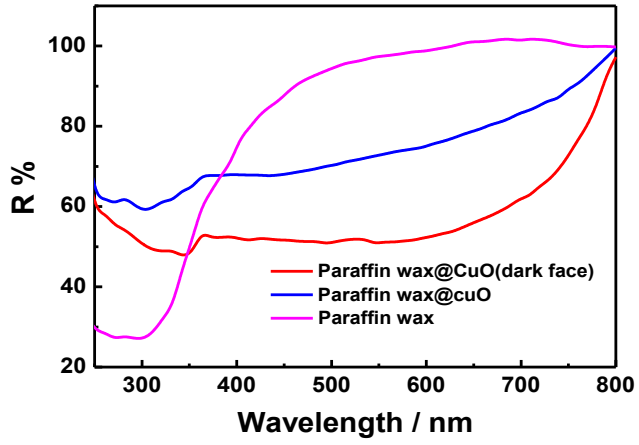

Fig. 5. Reflectance spectra of pure paraffin wax, nano-based paraffin wax (deep brown face), and nano-based paraffin wax.

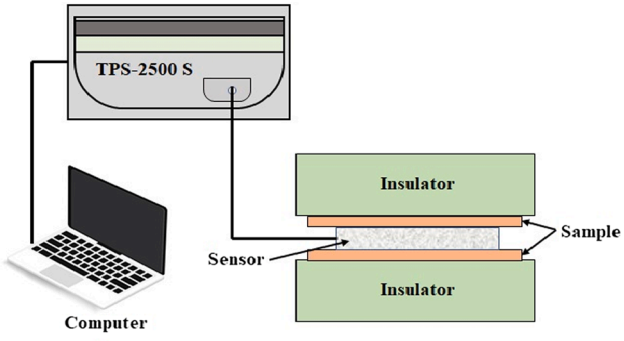

Fig. 6. Schematic of PCM thermal conductivity measurement via TPS analyzer.

form a 5 mm-thick layer in the basin. Also, a reservoir (capacity = 17 kg paraffin wax) was incorporated below the water basin to be utilized as a PCM container during the second and third cases of study. The thermo-physical properties of pure PCM and copper chips are given in Table 1. Besides, CuO nanoparticles were utilized to form the nanofluid (for all

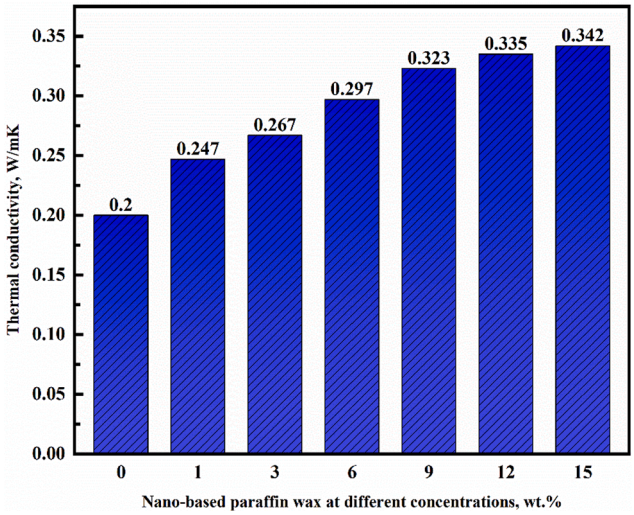

Fig. 7. Measured thermal conductivity of pure, and nano-based (at different concentrations) paraffin wax.

cases) and to be integrated with PCM (for the third case). In other words, the following three cases were proposed, conducted, and tested on the MDSSS:

Case I: Cu chips layer was immersed in CuO nanofluid (1% wt).
Case II: in addition to the previous combination, the PCM container was filled with 15 kg pure paraffin wax.
Case III: the pure PCM in case II was replaced by nano-based PCM (15% by mass CuO/paraffin wax).

3.2. Instrumentations and uncertainties

The SSs performance was evaluated based on the hourly recorded parameters, namely: solar radiation, wind speed, productivity amount, and temperatures of ambient, basin water, glass cover, and PCM. These parameters were measured via well-calibrated devices. The ranges and accuracies of the instrumentations were collected according to the manufacturers' data, whereas the errors were calculated according to Srithar (2003). The solar radiation intensity was measured via TES-133R (range = 0–2000 W/m^2, accuracy = ±10 W/m^2, and error = 1.5%). The wind speed was measured using commercial vane-type anemometer (range = 0.1– 30 m/s, accuracy = ±0.1 m/s, and error = 3.6%). Also, a calibrated flask (range = 0–2000 mL, accuracy = ±2 mL, and error = 0.5%) was utilized for collecting and scaling the yield. Finally, the various aforementioned temperatures were measured via K-type thermocouple and the readouts were monitored by a digital thermometer (range = −50 to 180 °C, accuracy = ±1°C, and error = 1.6%).

4. Thermo-economic performance calculation

The thermo-economic performance was evaluated to assure the benefits of the proposed modification from the thermal and economic points of view. For thermal performance, the energy and exergy efficiencies were evaluated based on the 1st and 2nd laws of thermodynamics, respectively. For the economic feasibility, the cost per unit liter of produced freshwater was estimated. The utilized formula for these estimations is presented in the following sub-sections.

4.1. Energy efficiency

According to the first law of thermodynamics, the daily thermal efficiency (η) is calculated as follows (Sharshir et al., 2017a):

$$\eta = \frac{\sum m_{ew} \times h_{fg}}{\sum I(t) \times A_s \times 3600} \quad (1)$$

as m_{ew} is hourly productivity, $I(t)$ is measured incident radiation, A_s area of evaporation and h_{fg} is water vapor latent heat which is assumed, on average within the temperature range, as 2325 kJ/(kg).

4.2. Exergy efficiency

The exergy or the 2nd law efficiency (η_{EX}) represents the ratio of the gained exergy ($E_{xoutput} = E_{xevap}$) due to evaporation to the input exergy (E_{xinput}=E_{xsun}) obtained from the sun (Sharshir et al., 2017a). These exergies can be obtained as follows:

$$E_{xoutput} = E_{xevap} = \frac{\dot{m_{ew}} \times h_{fg}}{(3600 s.h^{-1})} \times \left(1 - \frac{T_a}{T_w}\right) \quad (2)$$

where, T_a, T_w(K) are the temperatures of ambient air and water, respectively.

$$E_{x\,sun} = A_s \times I(t)_s \left[1 - \frac{4}{3} \times \left(\frac{T_a}{T_s}\right) + \frac{1}{3} \times \left(\frac{T_a}{T_s}\right)^4\right] \quad (3)$$

where T_s is the temperature of the sun (6000 K).

Then,

$$\eta_{EX} = \frac{\sum E_{x\,evap}}{\sum E_{x\,input}} \quad (4)$$

4.3. Cost evaluation

The benefit of the proposed modifications can be neglected if the production cost is high, even the gained efficiencies are high. Hence, it was necessary to evaluate the performance from an economic point of view. The cost per liter is calculated based on the annual total cost (*ATC*), which is a function of annual fixed cost (*AFC*), annual operational cost (*AOC*), annual maintenance cost (*AMC*), and annual salvage cost (*ASC*), as follows (Jaluria, 2019):

$$ATC = AFC + AOC + AMC - ASC \quad (5)$$

The values of ($AOC + AMC$) are considered as 20% of the total fixed cost (F) (El-Dessouky and Ettouney, 2002), and both *AFC* and *ASC* are functions of interest rate (i), and several operation years (n) as follows:

$$AFC = F \times \left[\frac{i(1+i)^n}{(1+i)^n - 1}\right] \quad (6)$$

$$ASC = S \times \left[\frac{i}{(1+i)^n - 1}\right] \quad (7)$$

assuming: S = 0.2F, i = 12%, and n = 10 years (Kabeel et al., 2010).

The production cost (*PC*) is a function of *ATC*, daily productivity (m_d), and number of operation days (N_d) as follows (Elshamy and El-Said, 2018):

$$PC = \frac{ATC}{m_d \times N_d} \quad (8)$$

where N_d is assumed to be 340 days/year (Elshamy and El-Said, 2018), respectively.

5. Results and discussions

The experiments were conducted simultaneously, under the same conditions, on both MDSSS (modified) and CSS (reference). Besides, based on resulted data, the thermo-economic performance was evaluated. Before employing the proposed additives, the conventional DSSS

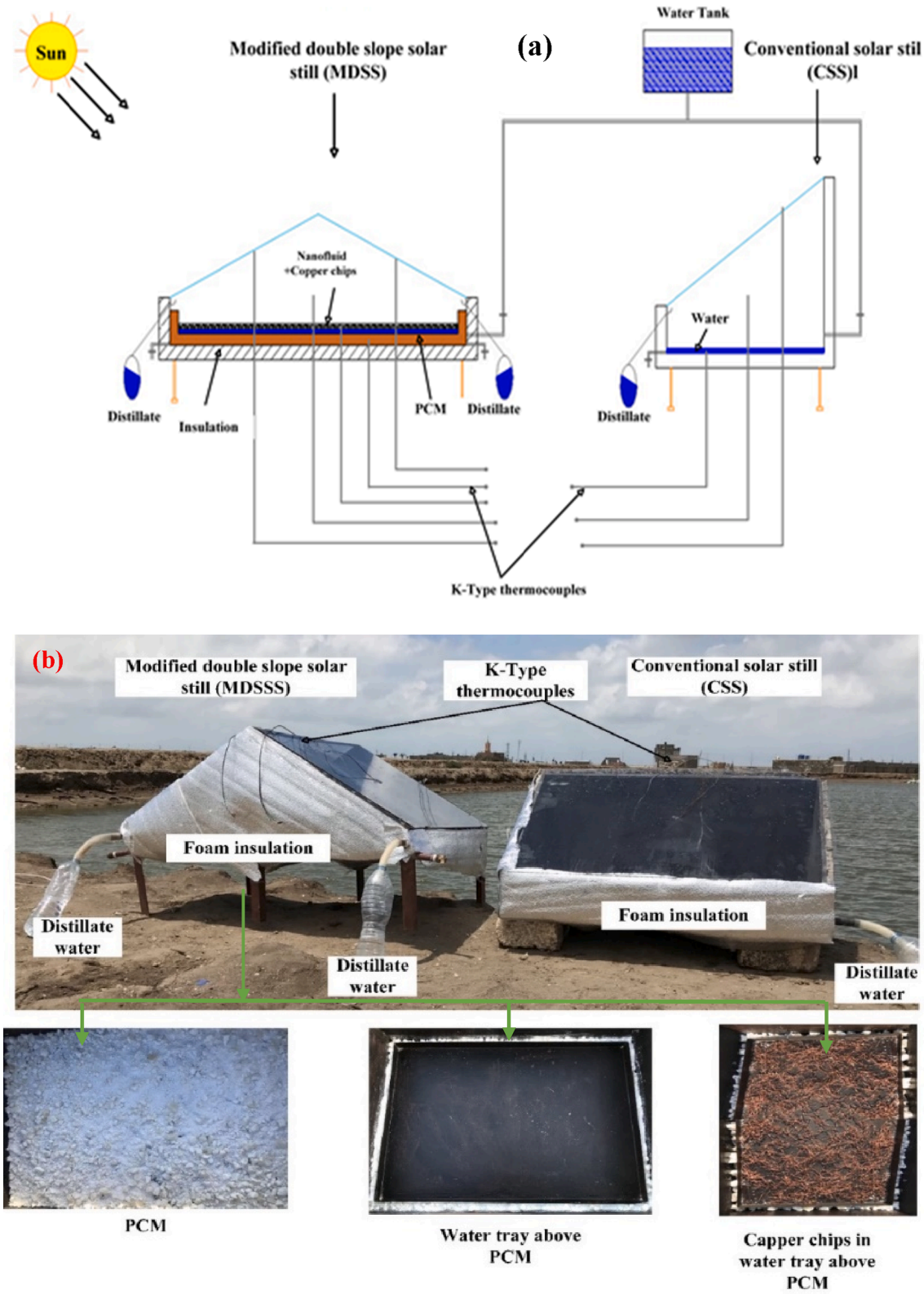

Fig. 8. Experimental setup: (a) Lay-out diagram, and (b) Photograph.

was investigated to determine the enhanced performance relative to CSS. In other words, the improvement obtained in yield and thermal performance due to changing the design from a single to double slope. Accordingly, the productivity of unmodified DSSS reached 3.5 L/m^2 defeating that of CSS by 14.5%. Beyond, the proposed additives were applied according to each case of study as mentioned in Section 3.1. The following subsections details introduce and discuss the resulted data based on the measured quantities. Each case was tested in more than one day, and the system showed good stability with semi-equal results and the herein presented data are for selected days as examples of illustration.

Table 1
Thermo-physical properties of paraffin wax and copper chips used.

Property	Value
Pure paraffin wax	
Density (Liquid/Solid), kg/m^3	760/818
Thermal conductivity, W/m.	0.24
Melting temperature,	56
Latent heat, kJ/kg	226
Specific heat capacity (Solid/Liquid), kJ/kg	2.95/2.51
Copper chips	
Density, kg/m^3	8960
Thermal conductivity, W/m	401
Specific heat capacity, kJ/kg	0.385

5.1. *Influence of copper chips immersed in CuO nanofluid: Case I*

Given, in Fig. 9, the recorded data during a whole diurnal experiment (8:00–18:00) in 25/07/2020. According to the meteorological data presented in Fig. 9(a), the ambient temperature and wind speed did not highly vary during the day. The air temperature was at the peak of 35 °C (at 14:00) with the daily average value of 32.2 °C. The wind speed fluctuated from 1.2 to 2.4 m/s, i.e., the average value was 1.8 m/s. On the other hand, according to each orientation (South for CSS, and East-West for MDSSS), the incident radiation followed the ordinary bell curve. For CSS, the incident radiation peak reached 980 W/m^2 at noon, starting from 350 W/m^2 at 8:00 and ending with 150 W/m^2 at 18:00. The daily average value of the incident radiation on the CSS cover was 583.2 W/m^2. For MDSSS, the peak values of incident radiation were 870 W/m^2 (at 11:00 am), and 830 W/m^2 (at 13:00), for the eastern and western covers, respectively.

The difference between water and glass temperatures can be considered as an indication of natural convection (vapor buoyancy). Besides, the higher the water temperature the higher vapor generation occurs. As presented in Fig. 9(b), the water temperature in the MDSSS was always higher than that of CSS, especially during the afternoon hours, and his superiority can be due to the thermal properties of copper chips and CuO nanoparticles. In other meaning, the copper chips have lower specific heat than water; hence they rapidly become warmer than water. Also, the thermal conductivity of copper chips is higher than that of water; hence the heat can be highly conducted to the nanofluid. Besides, it can be said that the copper chips worked as thermal storage material that conserved heat till the late (afternoon) hours. On the other hand, the nanofluid itself has higher thermal conductivity than that of pure water. All these benefits led to the superiority of the water temperature of MDSSS over that of CSS. As noticed, the water temperature reached, in maximum, about 75 and 68 °C for MDSSS, and CSS, respectively. As the glass cover temperature is influenced by vapor temperature, it was slightly higher for MDSSS than CSS, and its maximum value was 51 and 49 °C for MDSSS, and CSS, respectively.

Due to the aforementioned benefits that were obtained from the addition of copper chips and CuO nanofluid, the vapor generation and convection were enhanced, which can be noticed from the increased productivity, as shown in Fig. 9(c) and (d). The hourly productivity from MDSSS was always more than that of CSS, particularly at the afternoon

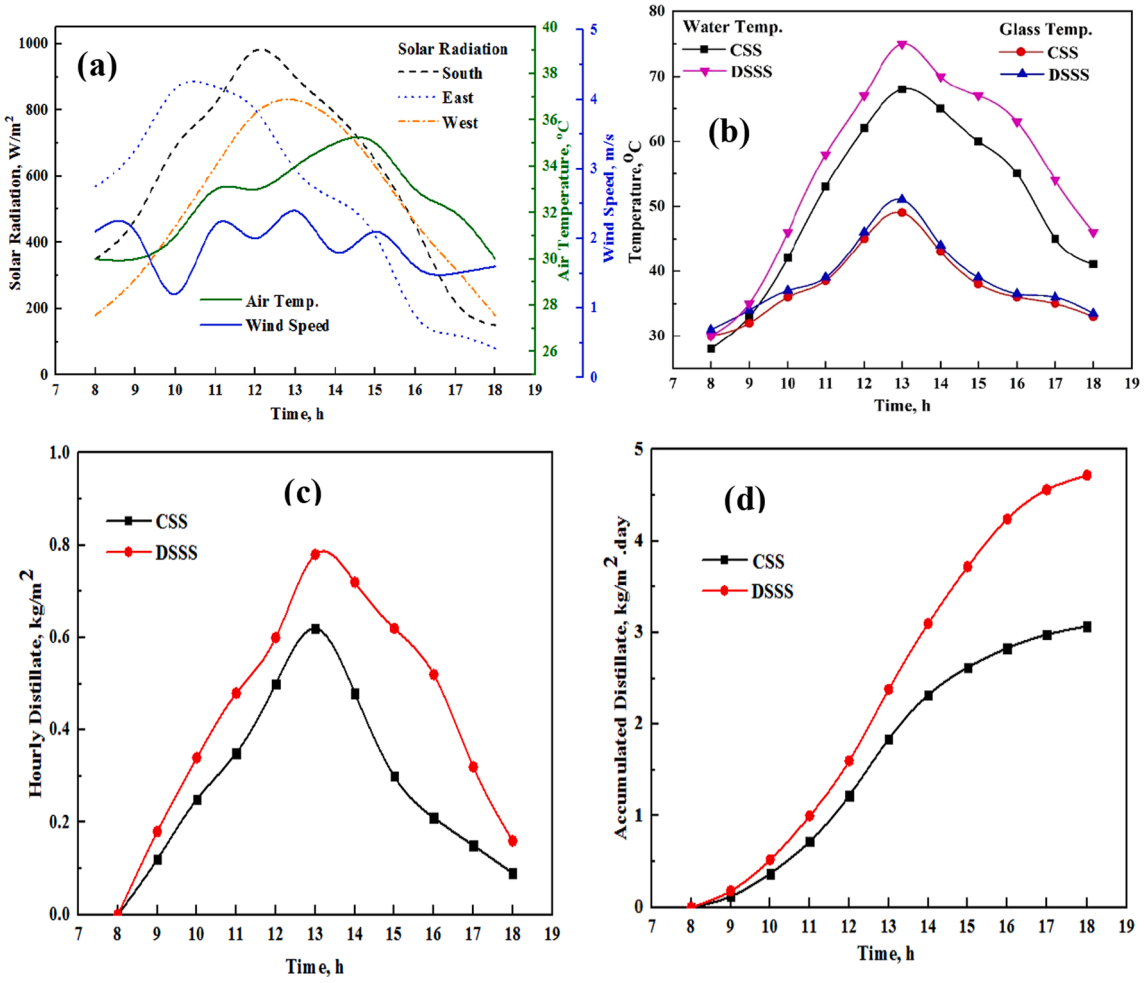

Fig. 9. Recorded parameters of case I for both MDSSS and CSS: (a) Meteorological data, (b) system (water and glass) temperatures, (c) hourly distillate, and (d) accumulated distillate.

hours, as noticed from Fig. 9(c). The maximum hourly yield was obtained from both SSs at 13:00 by the amount of 0.78 and 0.62 L/m^2 for MDSSS, and CSS, respectively. Additionally, as shown in Fig. 9(d), the accumulated production reached 4.72 and 3 L/m^2 for MDSSS, and CSS, respectively. In other meaning, the yield was enhanced by 54%.

5.2. *Influence of integrating pure PCM container in MDSSS with copper chips immersed in CuO nanofluid: Case II*

Herein, for the second case of study, the PCM container was employed besides the same additives of case I (copper chips and CuO nanofluid). Besides the obtained enhancements due to copper chips and CuO nanofluid, it was aimed that the presence of PCM can help in water heating and vapor generation during the low radiation periods (afternoon hours), and the system can last for some hours after sunset to get more productivity. That is to say that PCM can store thermal energy during the charging process till complete melting, then this heat can be a further help in increasing water temperature and continuing the vapor generation even with the reduction of solar radiation. For this aim, 15 kg of paraffin wax was contained in a rectangular tank below the basin of MDSSS.

The presented data, Fig. 10, was recorded on 05/08/2020 from 8:00 till reaching the cutoff of yield (thermal equilibrium conditions). As noticed, it was found that the thermal equilibrium occurred at 19:00 and 22:00 for CSS, and MDSSS, respectively. For the environmental data, shown in Fig. 10(a), the average values were close to that of the previous case with small variation due to the stability of the weather during the experimentation period. On the other hand, for system temperatures presented in Fig. 10(b), the superiority of water temperature in MDSSS over that of CSS was also noticed, and that is suggested due to the previously mentioned benefits obtained from both copper chips and CuO nanofluid. It was also noticed that the maximum water temperature of MDSSS was 76 °C recorded in delayed time (at 14:00) than that of CSS, which was 68.5 °C and obtained at 13:00. This delay occurred because of the presence of paraffin wax in MDSSS, as it requires more time for the phase change process (melting) extracting heat from basin water. Fortunately, the existence of copper chips and nanoparticles guaranteed that the water temperature in MDSSS did not fall below that of CSS even within the PCM charging process. For PCM behavior, the expected scenario of phase change material was obtained in which the temperature rose with absorbing sensible heat till melting point (56 °C), and then latent heat was extracted until reaching complete melting. Beyond, the wax liquid temperature continued to rise until the maximum value of 77 °C at 14:00 due to the addition of sensible heat, and became higher than that of basin water. Subsequently, with the reduction of solar radiation, the PCM lost heat (sensible heat) to water and worked as a heat source; hence the water temperature in MDSSS was stilled higher than that of CSS, therefore, the vapor generation was higher in MDSSS. Due to the discharging process and heat sored of PCM, the MDSSS take more time to reach the equilibrium state (till 22:00) and vapor continued in a generation, compared to CSS, which reached equilibrium at 19:00. For glass temperature, logically, MDSSS had higher values than CSS, and maximum values were 53 °C (at 14:00), and 50 °C (at 13:00), respectively.

Taking all the achieved benefits due to the presence of PCM, copper chips, and nanofluid, the production rate of MDSSS was higher than that of CSS, as shown in Fig. 10(c) and (d). The accumulated productivity of MDSSS reached 5.75 L/m^2 with an enhancement ratio of 83.7% w.r.t CSS.

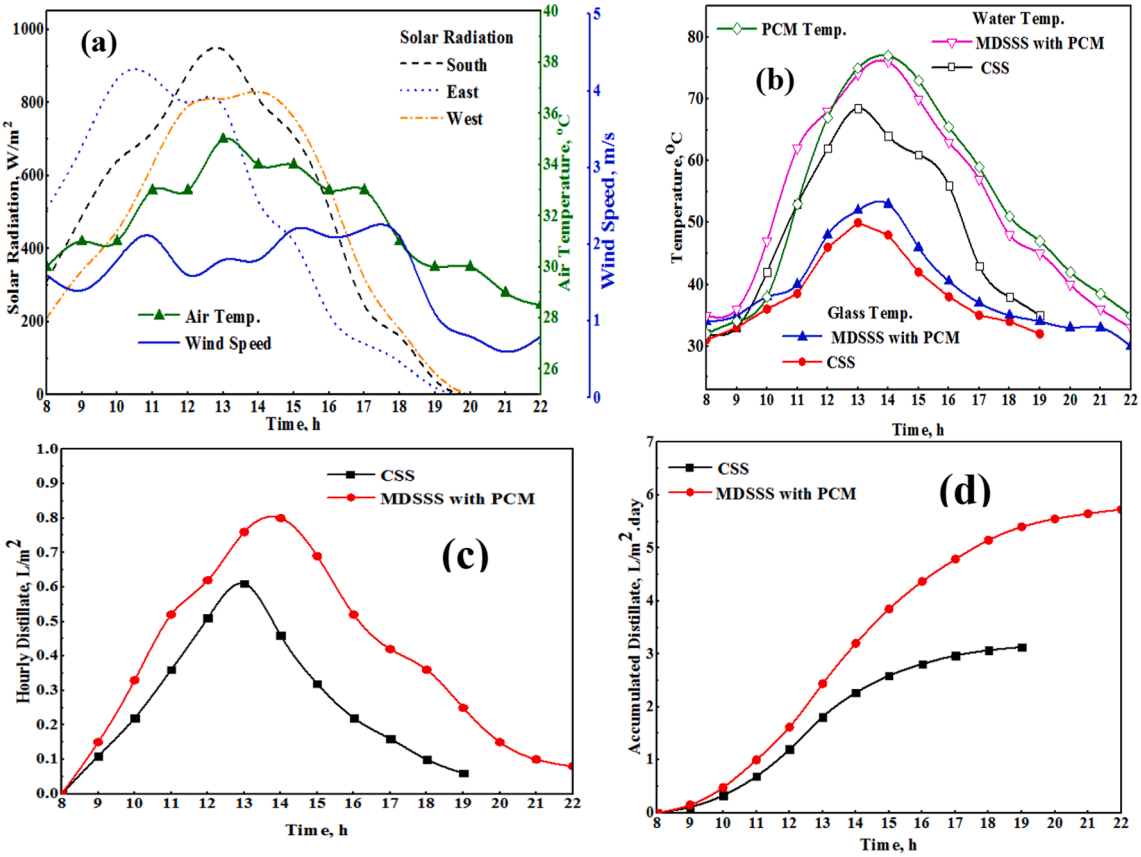

Fig. 10. Measured parameters of case II for both MDSSS and CSS: (a) Environmental data, (b) system (water, PCM, and glass) temperatures, (c) hourly productivity, and (d) accumulated productivity.

5.3. Influence of integrating nano-based PCM container in MDSSS with copper chips immersed in CuO nanofluid: Case III

The third case aimed to investigate the effect of alternating the previously used pure PCM with nano-based one. Hence, CuO nanoparticles were added to the paraffin wax pour with a mass concentration of 15% and added to the PCM container. The performance has experimented on 22/08/2020, which had close-similar meteorological conditions to the last two experiments. As shown in Fig. 11(a), the maximum values of ambient temperature and incident radiation from the south (CSS), east, and west (MDSSS) were 34 °C, and 935, 880, and 830 W/m^2, respectively. Also, as shown in Fig. 11(b), similar system behavior of Case II was obtained with increased values of its temperatures. The maximum values of water, PCM, and glass temperatures were 78, 79, and 53 °C, respectively, for MDSSS, whereas the maximum water and glass temperatures were 69 and 50 °C, respectively, for CSS. The increased values may be due to the improved thermal conductivity of PCM after the addition of CuO nanoparticles.

The increase in water temperature led to the enhancement of vapor generation, and hence, the productivity was enhanced, as shown in Fig. 11(c) and (d). The accumulated productivity reached 6.52 L/m^2 at 22:00 (equilibrium state), whereas the production of CSS reached equilibrium at 19:00 with 3.06 L/m^2, i.e., the yield was enhanced by 113%. As previously explained, the equilibrium state in MDSSS was delayed than that of CSS due to PCM thermal storage.

5.4. Thermo-economic performance of all cases

According to the experimental results, the thermal and economic performance was analyzed based on equations (1–8). For the thermal performance, the daily energetic and exegetic average efficiencies, and daily yield for both CSS and all cases proposed for MDSSS are given in Fig. 12. As noticed, the energy efficiency reached 32, 55, 63, and 68% for CSS, MDSSS at cases I, II, and III, respectively. In other meaning, it was enhanced, for MDSSS compared to CSS, by 72, 97, and 112.5% for cases I, II, and III, respectively. According to Eq. (1), with the same values of solar radiation, area, and latent heat, the energy efficiency varies proportionally with productivity, which was enhanced as previously illustrated. Also, due to the enhanced water temperature and productivity, the average daily exergy efficiency reached 3.5, 7.1, 8, and 9.8% for CSS, MDSSS at the case I, II, and III, respectively, i.e., it was improved by 110.3, 138.9, and 190% for DSSS at the cases I, II, and III, respectively, w.r.t CSS.

On the other hand, the proposed modifications proved good feasibility to be applied based on the economic analysis (cost per liter), as presented in Table 2. As given, the difference between the PC of all cases of MDSSS was very small (semi-equal), but also the values of F of these cases were low; hence, it can be said that applying the third case is feasible. The PC reached 0.017, and 0.013, 0.012, and 0.011 $/L for CSS, and MDSSS at cases I, II, and III, respectively. In other meaning, the freshwater production cost can be saved by 23.5, 29.4, and 35.3% for MDSSS at the case I, II, and III, respectively, w.r.t CSS.

Finally, based on comparing the current work results with these of other relevant works conducted in MDSSSs, the suggested improvements revealed acceptable thermo-economic performance as presented in Table 3.

6. Conclusions

This paper introduced a comprehensive investigation of modified double slope solar still (MDSSS) performance compared to conventional single slope solar still (CSS). Three additives were characterized and utilized as system modifications: copper chips, CuO nanoparticles/fluid, and paraffin wax as phase change material (PCM). Using these materials,

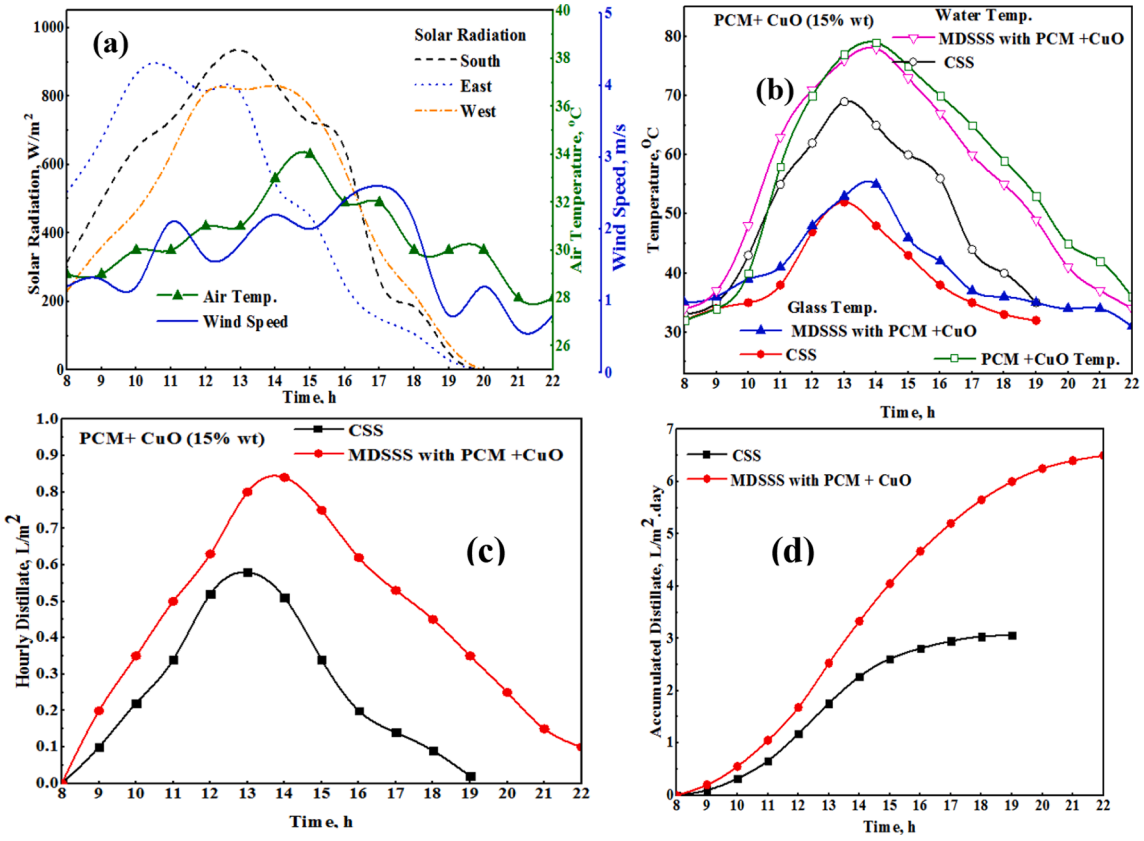

Fig. 11. Experimental data of case III for both MDSSS and CSS: (a) weather data, (b) system (water, nano-based PCM, and glass) temperatures, (c) hourly yield, and (d) accumulated yield.

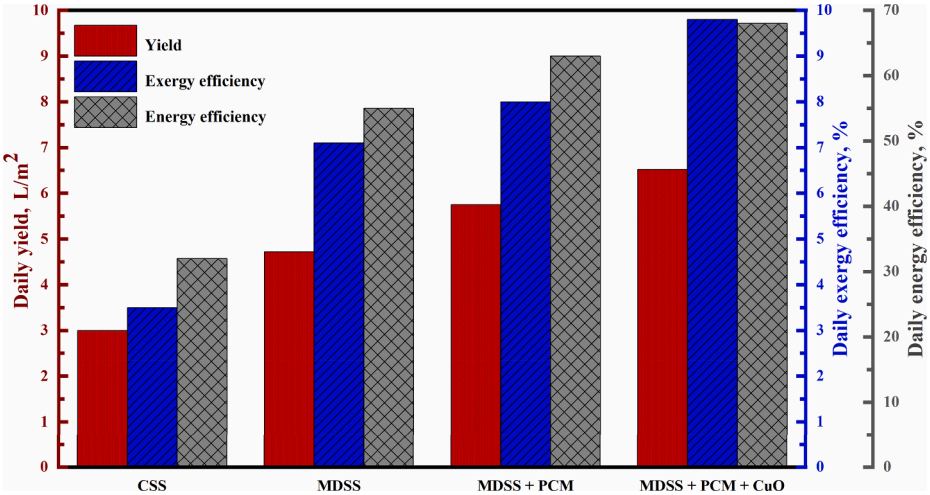

Fig. 12. Comparison of daily yield, exergy, and energy efficiencies among all cases.

Table 2
Economic parameters evaluation for the proposed systems.

Economic parameters	CSS	MDSSS (no PCM)	MDSSS (pure PCM)	MDSSS (nano-based PCM)
Total fixed cost, $	85	100	112	120
Annual salvage cost, $/year	0.96	1.13	1.27	1.36
Annual fixed cost, $/year	15.04	17.7	19.82	21.23
Annual maintenance cost, $/year	3.00	3.53	3.96	4.24
Averaged water productivity L/day	2.8	4.5	5.5	6.3
Annual water productivity L/m^2. year	952	1530	1870	2142
Annual total cost, $/year	17.08	20.098	22.51	24.11
Cost of distilled water, $/L	0.017	0.013	0.012	0.011

Table 3
Comparison of current work with other relevant studies conducted on MDSSS.

Reference	Modification	Accumulated productivity (L/m^2)	Efficiency (%)	Cost per liter ($/L)
Current work	Case I	4.72	56	0.013
	Case II	5.75	63	0.012
	Case III	6.52	68	0.011
(Morad et al., 2015)	Active SS with flat plate collector and cooling glass cover	7.8	57.1	–
(Elmaadawy et al., 2020a)	CB nanoparticles dispersed on the top of black wick/ gravel/foam layers	4.91	59.47	0.0147
(Sharshir,et al., 2020e)	Stepped basin with carbon black nanoparticles dispersed on linen wick	4.46	60.2	0.018
(Muthu Saravanan et al., 2020)	Using kanchey marbles as sensible heat storage materials	4.1	–	–
(Gnanaraj and Velmurugan, 2019)	Finned corrugated basin, black granite, wick, and external reflectors	5.13	76	Rs.1.62

three cases were experimented on MDSSS: case I (copper chips immersed in CuO/water nanofluid (1.5 wt%), case II (case I + pure PCM container below the water basin), and case III (case I + nano-based PCM, 15 wt%, container below the water basin). Moreover, the thermal performance was analyzed based on efficiencies of the first and second laws of thermodynamics, and economic analysis was conducted to calculate the freshwater production cost. The following results can be concluded:

- From thermo-physical characterization, using CuO nanoparticles increased the thermal conductivity of water and PCM with negligible change in their specific heat. Additionally, the copper chips had high thermal conductivity with lower specific heat than water; therefore, the water temperature and vapor generation rapidly increased.
- Case III obtained the highest enhancement from both production and thermo-economic points of view.
- The yield of MDSSS was higher than that of CSS by 54, 83.7, and 113% for case I, case II, and case III, respectively.
- The energy and exergy efficiencies of MDSSS were higher than that of CSS and their enhancement ratios reached (72, and 110.3%), (97, and 138.9%), and (112.5, and 190%) for the case I, case II, and case III, respectively.
- The freshwater unit (liter) cost was about the same value for all cases of MDSSS, and the saving ratio reached 35.3% for case III w.r.t. CSS.

Declaration of Competing Interest

The authors declare that they have no known competing financial interests or personal relationships that could have appeared to influence the work reported in this paper.

Acknowledgement

The work was sponsored by National Key Research and Development Program of China (2018YFE0127800),National Natural Science Foundation of China (51950410592) and Fundamental Research Funds for the Central Universities (2019kfyRCPY045) and Program for HUST Academic Frontier Youth Team. The authors thank the National Supercomputing Center in Tianjin (NSCC-TJ) and China Scientific Computing Grid (ScGrid) for assisting in computations. Also, this paper is based upon work supported by Science, Technology & Innovation Funding Authority (STIFA), Egypt and China, under grant (40517).

References

Abdallah, S., Badran, O., 2008. Sun tracking system for productivity enhancement of solar still. Desalination 220 (1–3), 669–676.

Abdelaziz, G.B., El-Said, E.M.S., Bedair, A.G., Sharshir, S.W., Kabeel, A.E., Elsaid, A.M., 2021. Experimental study of activated carbon as a porous absorber in solar desalination with environmental, exergy, and economic analysis. Process Saf. Environ. Prot. 147, 1052–1065.
Abdelgaied, M., Kabeel, A.E., Kandeal, A.W., Abosheiasha, H.F., Shalaby, S.M., Hamed, M.H., Yang, N., Sharshir, S.W., 2021. Performance assessment of solar PV-driven hybrid HDH-RO desalination system integrated with energy recovery units and solar collectors: Theoretical approach. Energy Convers. Manage. 239, 114215.
Abujazar, M.S.S., Fatihah, S., Ibrahim, I.A., Kabeel, A.E., Sharil, S., 2018. Productivity modelling of a developed inclined stepped solar still system based on actual performance and using a cascaded forward neural network model. J. Cleaner Prod. 170, 147–159.
Ali, H., 1991. Experimental study on air motion effect inside the solar still on still performance. Energy Convers. Manage. 32 (1), 67–70.
Alsehli, M., Choi, J.-K., Aljuhan, M., 2017. A novel design for a solar powered multistage flash desalination. Sol. Energy 153, 348–359.
Arunkumar, T., Kabeel, A.E., Raj, K., Denkenberger, D., Sathyamurthy, R., Ragupathy, P., Velraj, R., 2018. Productivity enhancement of solar still by using porous absorber with bubble-wrap insulation. J. Cleaner Prod. 195, 1149–1161.
Bendfeld, J., Broker, C., Menne, K., Ortjohann, E., Temme, L., Vob, J., Carvallo, P., 1998. Design of a PV-powered reverse osmosis plant for desalination of brackish water, Proceedings of 2nd world conference and exhibition on photovoltaic solar energy conversion, Vienna, Austria. pp. 3075–3077.
Choi, S.U., Eastman, J.A., 1995. Enhancing thermal conductivity of fluids with nanoparticles. Argonne National Lab, IL (United States).
Dsilva Winfred Rufuss, D., Suganthi, L., Iniyan, S., Davies, P.A., 2018. Effects of nanoparticle-enhanced phase change material (NPCM) on solar still productivity. J. Cleaner Prod. 192, 9–29.
El-Dessouky, H.T., Ettouney, H.M., 2002. Fundamentals of Salt Water Desalination. Elsevier.
El-Sebaii, A., Al-Ghamdi, A., Al-Hazmi, F., Faidah, A.S., 2009. Thermal performance of a single basin solar still with PCM as a storage medium. Appl. Energy 86 (7–8), 1187–1195.
El-Shafai, N.M., Abdelfatah, M.M., El-Khouly, M.E., El-Mehasseb, I.M., El-Shaer, A., Ramadan, M.S., Masoud, M.S., El-Kemary, M.A., 2020. Magnetite nano-spherical quantum dots decorated graphene oxide nano sheet (GO@ Fe3O4): Electrochemical properties and applications for removal heavy metals, pesticide and solar cell. Appl. Surf. Sci. 506, 144896.
El-Shafai, N.M., Ji, R., Abdelfatah, M., Hamada, M.A., Kandeal, A.W., El-Mehasseb, I.M., El-Shaer, A., An, M., Ramadan, M.S., Sharshir, S.W., Ismail, W., 2021. Investigation of a novel (GO@CuO.γ-Al2O3) hybrid nanocomposite for solar energy applications. J. Alloy. Compd. 856, 157463.
Elango, T., Kannan, A., Murugavel, K.K., 2015. Performance study on single basin single slope solar still with different water nanofluids. Desalination 360, 45–51.
Elkadeem, M.R., Kotb, K.M., Elmaadawy, K., Ullah, Z., Elmolla, E., Liu, B., Wang, S., Dán, A., Sharshir, S.W., 2021. Feasibility analysis and optimization of an energy-water-heat nexus supplied by an autonomous hybrid renewable power generation system: an empirical study on airport facilities. Desalination 504, 114952.
Elmaadawy, K., Kandeal, A.W., Khalil, A., Elkadeem, M.R., Liu, B., Sharshir, S.W., 2020a. Performance improvement of double slope solar still via combinations of low cost materials integrated with glass cooling. Desalination, 114856.
Elmaadawy, K., Kotb, K.M., Elkadeem, M.R., Sharshir, S.W., Dán, A., Moawad, A., Liu, B., 2020b. Optimal sizing and techno-enviro-economic feasibility assessment of large-scale reverse osmosis desalination powered with hybrid renewable energy sources. Energy Convers. Manage. 224, 113377.
Elshamy, S.M., El-Said, E.M., 2018. Comparative study based on thermal, exergetic and economic analyses of a tubular solar still with semi-circular corrugated absorber. J. Cleaner Prod. 195, 328–339.
Elsheikh, A.H., Sharshir, S.W., Ahmed Ali, M.K., Shaibo, J., Edreis, E.M.A., Abdelhamid, T., Du, C., Haiou, Z., 2019. Thin film technology for solar steam generation: a new dawn. Sol. Energy 177, 561–575.
Gnanaraj, S.J.P., Velmurugan, V., 2019. An experimental study on the efficacy of modifications in enhancing the performance of single basin double slope solar still. Desalination 467, 12–28.
Hamed, M.H., Kabeel, A.E., Omara, Z.M., Sharshir, S.W., 2015. Mathematical and experimental investigation of a solar humidification–dehumidification desalination unit. Desalination 358, 9–17.
Hassan, H., Abo-Elfadl, S., 2017. Effect of the condenser type and the medium of the saline water on the performance of the solar still in hot climate conditions. Desalination 417, 60–68.
Jaluria, Y., 2019. Design and Optimization of Thermal Systems: with MATLAB Applications. CRC Press.
Kabeel, A.E., Abdelgaied, M., 2016. Improving the performance of solar still by using PCM as a thermal storage medium under Egyptian conditions. Desalination 383, 22–28.
Kabeel, A.E., Abdelgaied, M., Eisa, A., 2018. Enhancing the performance of single basin solar still using high thermal conductivity sensible storage materials. J. Cleaner Prod. 183, 20–25.
Kabeel, A.E., El-Maghlany, W.M., Abdelgaied, M., Abdel-Aziz, M.M., 2020. Performance enhancement of pyramid-shaped solar stills using hollow circular fins and phase change materials. J. Storage Mater. 31, 101610.
Kabeel, A.E., Hamed, A.M., El-Agouz, S.A., 2010. Cost analysis of different solar still configurations. Energy 35 (7), 2901–2908.
Kabeel, A.E., Hamed, M.H., Omara, Z.M., Sharshir, S.W., 2013. Water desalination using a humidification-dehumidification technique. A detailed review. J. Natural Resour. 4 (3), 20.
Kabeel, A.E., Hamed, M.H., Omara, Z.M., Sharshir, S.W., 2014. Experimental study of a humidification-dehumidification solar technique by natural and forced air circulation. Energy 68, 218–228.
Kabeel, A.E., Sathyamurthy, R., Sharshir, S.W., Muthumanokar, A., Panchal, H., Prakash, N., Prasad, C., Nandakumar, S., El Kady, M.S., 2019. Effect of water depth on a novel absorber plate of pyramid solar still coated with TiO2 nano black paint. J. Cleaner Prod. 213, 185–191.
Kabeel, A.E., Teamah, M.A., Abdelgaied, M., Abdel Aziz, G.B., 2017. Modified pyramid solar still with v-corrugated absorber plate and PCM as a thermal storage medium. J. Cleaner Prod. 161, 881–887.
Khare, V.R., Singh, A.P., Kumar, H., Khatri, R., 2017. Modelling and Performance Enhancement of Single Slope Solar Still Using CFD. Energy Procedia 109, 447–455.
Kotb, K.M., Elkadeem, M.R., Khalil, A., Imam, S.M., Hamada, M.A., Sharshir, S.W., Dán, A., 2021. A fuzzy decision-making model for optimal design of solar, wind, diesel-based RO desalination integrating flow-battery and pumped-hydro storage: case study in Baltim, Egypt. Energy Convers. Manage. 235, 113962.
Lanje, A.S., Sharma, S.J., Pode, R.B., Ningthoujam, R.S., 2010. Synthesis and optical characterization of copper oxide nanoparticles. Adv. Appl. Sci. Res. 1 (2), 36–40.
Madani, A.A., Zaki, G.M., 1995. Yield of solar stills with porous basins. Appl. Energy 52 (2), 273–281.
Morad, M.M., El-Maghawry, H.A.M., Wasfy, K.I., 2015. Improving the double slope solar still performance by using flat-plate solar collector and cooling glass cover. Desalination 373, 1–9.
Mousa, H., Gujarathi, A.M., 2016. Modeling and analysis the productivity of solar desalination units with phase change materials. Renew. Energy 95, 225–232.
Muthu Saravanan, N., Rajakumar, S., Moshi, A.A.M., 2020. Experimental investigation on the performance enhancement of single basin double slope solar still using kanchey marbles as sensible heat storage materials. Mater. Today: Proc.
Nafey, A., Abdelkader, M., Abdelmotalip, A., Mabrouk, A., 2001. Solar still productivity enhancement. Energy Convers. Manage. 42 (11), 1401–1408.
Patel, S.K., Kumar, B., Pal, P., Dev, R., Singh, D., 2020. Production of potable water from Gomti River by using modified double slope solar still with external mounted reflectors. Sol. Energy 209, 576–589.
Peng, G., Deng, S., Sharshir, S.W., Ma, D., Kabeel, A.E., Yang, N., 2020. High efficient solar evaporation by airing multifunctional textile. Int. J. Heat Mass Transf. 147, 118866.
Peng, G., Ding, H., Sharshir, S.W., Li, X., Liu, H., Ma, D., Wu, L., Zang, J., Liu, H., Yu, W., Xie, H., Yang, N., 2018. Low-cost high-efficiency solar steam generator by combining thin film evaporation and heat localization: Both experimental and theoretical study. Appl. Therm. Eng. 143, 1079–1084.
Peng, G., Sharshir, S.W., Wang, Y., An, M., Ma, D., Zang, J., Kabeel, A.E., Yang, N., 2021. Potential and challenges of improving solar still by micro/nano-particles and porous materials – a review. J. Cleaner Prod. 311, 127432.
Rababa'h, H.M., 2003. Experimental study of a solar still with sponge cubes in basin. Energy Convers. Manage. 44(9), 1411–1418.
Radhwan, A.M., 2005. Transient performance of a stepped solar still withbuilt-in latent heat thermal energy storage. Desalination 171 (1), 61–76.
Rashidi, S., Akar, S., Bovand, M., Ellahi, R., 2018. Volume of fluid model to simulate the nanofluid flow and entropy generation in a single slope solar still. Renew. Energy 115, 400–410.
Samuel Hansen, R., Kalidasa Murugavel, K., 2017. Enhancement of integrated solar still using different new absorber configurations: an experimental approach. Desalination 422, 59–67.
Sathyamurthy, R., Kabeel, A.E., Balasubramanian, M., Devarajan, M., Sharshir, S.W., Manokar, A.M., 2020. Experimental study on enhancing the yield from stepped solar still coated using fumed silica nanoparticle in black paint. Mater. Lett. 272, 127873.
Shalaby, S.M., El-Bialy, E., El-Sebaii, A.A., 2016. An experimental investigation of a v-corrugated absorber single-basin solar still using PCM. Desalination 398, 247–255.
Sharshir, S., Elsheikh, A., Peng, G., Yang, N., El-Samadony, M., Kabeel, A., 2017a. Thermal performance and exergy analysis of solar stills–a review. Renew. Sustain. Energy Rev. 73, 521–544.
Sharshir, S.W., Abd Elaziz, M., Elkadeem, M.R., 2020a. Enhancing thermal performance and modeling prediction of developed pyramid solar still utilizing a modified random vector functional link. Sol. Energy 198, 399–409.
Sharshir, S.W., Algazzar, A.M., Elmaadawy, K.A., Kandeal, A.W., Elkadeem, M.R., Arunkumar, T., Zang, J., Yang, N., 2020b. New hydrogel materials for improving solar water evaporation, desalination and wastewater treatment: a review. Desalination 491, 114564.
Sharshir, S.W., El-Shafai, N.M., Ibrahim, M.M., Kandeal, A.W., El-Sheshtawy, H.S., Ramadan, M.S., Rashad, M., El-Mehasseb, I.M., 2021. Effect of copper oxide/cobalt oxide nanocomposite on phase change material for direct/indirect solar energy applications: Experimental investigation. J. Storage Mater. 38, 102526.
Sharshir, S.W., Elkadeem, M.R., Meng, A., 2020c. Performance enhancement of pyramid solar distiller using nanofluid integrated with v-corrugated absorber and wick: an experimental study. Appl. Therm. Eng. 168, 114848.
Sharshir, S.W., Ellakany, Y.M., Algazzar, A.M., Elsheikh, A.H., Elkadeem, M.R., Edreis, E. M.A., Waly, A.S., Sathyamurthy, R., Panchal, H., Elashry, M.S., 2019a. A mini review of techniques used to improve the tubular solar still performance for solar water desalination. Process Saf. Environ. Prot. 124, 204–212.
Sharshir, S.W., Ellakany, Y.M., Eltawil, M.A., 2020d. Exergoeconomic and environmental analysis of seawater desalination system augmented with nanoparticles and cotton hung pad. J. Cleaner Prod. 248, 119180.
Sharshir, S.W., Elsheikh, A.H., Edreis, E., Ali, M.K.A., Sathyamurthy, R., Kabeel, A., Zang, J., Yang, N.J.D.W.T., 2019c. Improving the solar still performance by using thermal energy storage materials: A review of recent developments. Desalin Water Treat. 165, 1–15.

Sharshir, S.W., Elsheikh, A.H., Ellakany, Y.M., Kandeal, A.W., Edreis, E.M.A., Sathyamurthy, R., Thakur, A.K., Eltawil, M.A., Hamed, M.H., Kabeel, A.E., 2020g. Improving the performance of solar still using different heat localization materials. Environ. Sci. Pollut. Res. 27 (11), 12332–12344.

Sharshir, S.W., Eltawil, M.A., Algazzar, A.M., Sathyamurthy, R., Kandeal, A.W., 2020e. Performance enhancement of stepped double slope solar still by using nanoparticles and linen wicks: Energy, exergy and economic analysis. Appl. Therm. Eng. 174, 115278.

Sharshir, S.W., Kandeal, A.W., Ismail, M., Abdelaziz, G.B., Kabeel, A.E., Yang, N., 2019b. Augmentation of a pyramid solar still performance using evacuated tubes and nanofluid: experimental approach. Appl. Therm. Eng. 160, 113997.

Sharshir, S.W., Peng, G., Elsheikh, A.H., Edreis, E.M.A., Eltawil, M.A., Abdelhamid, T., Kabeel, A.E., Zang, J., Yang, N., 2018. Energy and exergy analysis of solar stills with micro/nano particles: a comparative study. Energy Convers. Manage. 177, 363–375.

Sharshir, S.W., Peng, G., Elsheikh, A.H., Eltawil, M.A., Elkadeem, M.R., Dai, H., Zang, J., Yang, N., 2020f. Influence of basin metals and novel wick-metal chips pad on the thermal performance of solar desalination process. J. Cleaner Prod. 248, 119224.

Sharshir, S.W., Peng, G., Wu, L., Essa, F.A., Kabeel, A.E., Yang, N., 2017b. The effects of flake graphite nanoparticles, phase change material, and film cooling on the solar still performance. Appl. Energy 191, 358–366.

Sharshir, S.W., Peng, G., Wu, L., Yang, N., Essa, F.A., Elsheikh, A.H., Mohamed, S.I.T., Kabeel, A.E., 2017c. Enhancing the solar still performance using nanofluids and glass cover cooling: Experimental study. Appl. Therm. Eng. 113, 684–693.

Sharshir, S.W., Peng, G., Yang, N., El-Samadony, M.O.A., Kabeel, A.E., 2016a. A continuous desalination system using humidification – dehumidification and a solar still with an evacuated solar water heater. Appl. Therm. Eng. 104, 734–742.

Sharshir, S.W., Peng, G., Yang, N., Eltawil, M.A., Ali, M.K.A., Kabeel, A.E., 2016b. A hybrid desalination system using humidification-dehumidification and solar stills integrated with evacuated solar water heater. Energy Convers. Manage. 124, 287–296.

Sharshir, S.W., Yang, N., Peng, G., Kabeel, A.E., 2016c. Factors affecting solar stills productivity and improvement techniques: A detailed review. Appl. Therm. Eng. 100, 267–284.

Srithar, K., 2003. Studies on solar augmented evaporation systems for tannery effluent (Soak liquor). PhD thesis. Indian Institute of Technology, Madras.

Su, W., Darkwa, J., Kokogiannakis, G., 2015. Review of solid–liquid phase change materials and their encapsulation technologies. Renew. Sustain. Energy Rev. 48, 373–391.

Tanaka, H., Nakatake, Y., 2009. Increase in distillate productivity by inclining the flat plate external reflector of a tilted-wick solar still in winter. Sol. Energy 83 (6), 785–789.

Thakur, A.K., Sathyamurthy, R., Sharshir, S.W., Elnaby Kabeel, A., Shamsuddin Ahmed, M., Hwang, J.-Y., 2021. A novel reduced graphene oxide based absorber for augmenting the water yield and thermal performance of solar desalination unit. Mater. Lett. 286, 128867.

Thimmaraju, M., Sreepada, D., Babu, G.S., Dasari, B.K., Velpula, S.K., Vallepu, N., 2018 Sep 19. Desalination of water. Desalin Water Treat., pp. 333–347.

Voropoulos, K., Mathioulakis, E., Belessiotis, V., 2003. Solar stills coupled with solar collectors and storage tank—analytical simulation and experimental validation of energy behavior. Sol. Energy 75 (3), 199–205.

Wang, Y., Kandeal, A.W., Swidan, A., Sharshir, S.W., Abdelaziz, G.B., Halim, M.A., Kabeel, A.E., Yang, N., 2020. Prediction of tubular solar still performance by machine learning integrated with Bayesian optimization algorithm. Appl. Therm. Eng., 116233